VALIDATION APPROACH FOR A SPATIALLY AND TEMPORALLY RESOLVED FAULT ARC MODEL

F. Mingers*, T. Ballweber, S. Kimpeler, A. Moser

IAEW at RWTH Aachen University, Aachen, 52062, Germany

* f.mingers@iaew.rwth-aachen.de

Abstract. This paper presents a method to validate arc models for fault arc applications by examining the effect of changed boundary conditions on arc parameters, e.g. voltage and pressure build-up. The study shows the impact of ignition location on arc voltage and pressure build-up and prediction accuracy of the presented model. The results indicate insufficient accuracy in predicting arc voltage during dynamic phases, while the pressure build-up prediction aligns well with the experimental results.

Keywords: alternating current arcs, fault arc simulation, plasma, polymer ablation, switchgear.

1. Introduction

The behavior of fault arcs in switchgear has long been in the focus of research with regards to the operational safety of the equipment. Due to core temperatures of several thousand Kelvin and arc dynamics, there are influencing phenomena, such as energy conversion into mass ablation and pressure build-up, which cannot be measured reliably and time-resolved. However, these phenomena have a significant impact on the arc behavior and therefore on operational safety and passive fault arc protection.

Considering the advancements in computing power, spatially and temporally resolved arc models provide the opportunity to reduce efforts on experimental investigation and enhance the understanding of fault arcs through computational fluid dynamics (CFD) approaches. Furthermore, simulations can be used to optimize the design of switchgear subject to passive protection measures, e.g. by predicting the movement of the arc. This requires the simulation to accurately depict arc behavior, including the arc voltage, arc movement, converted energy, and the energy involved in material ablation, and pressure build-up. As most of the investigation have been carried out on switching arcs (see, e.g., [1, 2]), it is necessary to asses the applicability for fault arcs. This process involves considering experimental and simulation studies to parameterize the included models and identify the fault arc behavior encompassing aforementioned characteristics. Initial investigation were conducted by Rümpler [3] and Singh [4]. It is necessary to develop an experimental setup enabling systematic investigation on the various aspects and influencing factors associated with arcing phenomena, while ensuring replicable results.

In this paper an experimental setup is presented that allows the investigation of fault arcs and the influence of altered boundary conditions on arc behavior, which can be further used for the validation of fault arc simulations. Moreover, the parameter space that can be covered within the setup is defined and the influence of altered boundary conditions is shown by means of exemplary results. Finally, the numerical model is presented and the simulation results are compared with the experimental results.
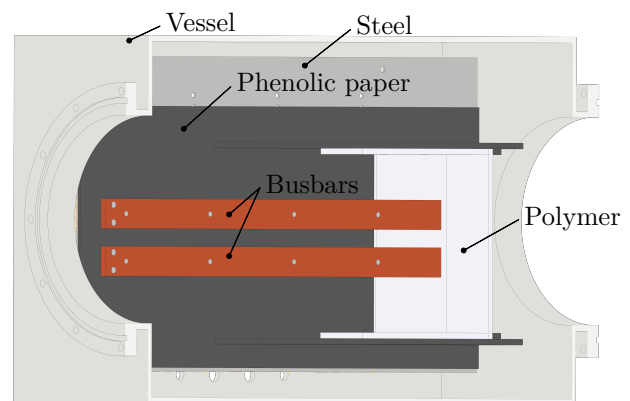
2. Method

Figure 1. Half-section of the pressure-tight vessel for investigation of fault arc behavior on parallel busbars

The experimental setup for investigating fault arcs consists of two copper busbars with rectangular section enclosed in a hermetically sealed, pressure-tight vessel with a volume of approximately 380 l (cf. Figure 1). Two bushings connect the busbars to the electrical circuit through the left enclosure wall. A thin copper wire ($A_{\text{Wire}} = 0.1\,\text{mm}^2$; $R = 0.6\,\Omega/\text{m}$) is used to ignite the arc, which is attached onto the busbars. The end part of the busbars is surrounded on four sides by replaceable plates (here: polymer) to imitate different materials in switchgear.

The setup is designed to ensure a high level of comparability between each test with the same parameterization. Table 1 shows the variation parameters and their corresponding ranges. By adjusting the positions of the insulators, the distance between the busbars (d_{bb}) can be varied. The available volume for the fault arc at the busbar ends, which affects magnetic widening

Parameter	Symbol	Variation
Gap busbars	d_{bb}	$[0.01, 0.07]\,\mathrm{m}$
Gap busbar/ end plate	d_{be}	$[0.0, 0.09]\,\mathrm{m}$
Ignition location	x_{ign}	$\{0.08, 0.8\}\,\mathrm{m}$
Initial pressure	p_0	$\{0.5, 3.0\}\,\mathrm{bar}$
Polymer material	−	−
Electrode material	−	−

Table 1. Parameter space of the experimental setup and the corresponding variation ranges

and determines the distance of the initial arc between the busbars and the polymer, can be adjusted by varying the distance between the busbars and the end plate, denoted as d_{be}. The current flow through the busbars and the arc creates a magnetic field resulting in Lorentz forces driving the arc between the busbars towards the polymer plates. By changing the position of ignition (x_{ign}) the traveling distance of the arc can be varied. With $x_{\mathrm{ign}} = 0\,\mathrm{m}$ marking the in-feed location on the left side of the setup. The structure of the internal components allows for changing polymers and busbars materials.

Before and after each test series, which consists of three repetitions, the polymer plates are cleaned of soot with an alcohol-based solution and afterwards weighed. Potential copper droplets attached onto the surface are removed beforehand.

2.1. Test Circuit

The energy required to feed the fault arc is provided by a capacitor bank with a total capacity of $C_{\mathrm{HC}} = 17.0\,\mathrm{mF}$. The power supply is designed as a damped *LC* resonance circuit with an inductance of $L_{\mathrm{HC}} = 0.63\,\mathrm{mH}$, a current frequency of approximately $47.9\,\mathrm{Hz}$, and the maximum charging voltage of the capacitors at $8\,000\,\mathrm{V}$. The peak short circuit current is about $26\,\mathrm{kA}$ (cf. Figure 2). This results in a stiff current source, whereby an impressed current can be assumed.

Current measurement is carried out seperately on the earthed busbar and the earthed vessel using two Rogowski coil current probes, allowing the potential current flowing through the enclosure during a flashover to be measured. The injected current is obtained as the sum of both currents. An active differential probe (divider ratio of $1 : 1\,000$) is used to measure the arc voltage between the high voltage and the earthed busbar. Pressure build-up in the closed enclosure is measured using a piezoelectric pressure sensor (sensitivity of $-36.89\,\mathrm{pC/bar}$) integrated into the frontwall of the vessel.The pressure measurement is filtered with a 3rd order Savitzky-Golay-Filter. The arc power and the total energy converted are calculated from the current and voltage course. A scale (with a deviation of $0.01\,\mathrm{g}$) is used to determine the amount of ablated polymer material.

2.2. Modeling of the fault arc

To model the arc as thermal plasma under the assumption of local thermodynamic equilibrium, the conservation equations for mass (1), momentum (2), and energy (3) are utilized as follows:

$$\frac{\partial \rho}{\partial t} + \nabla \left(\rho \mathbf{v}\right) = 0, \tag{1}$$

$$\frac{\partial \left(\rho \mathbf{v}\right)}{\partial t} + \nabla \left(\rho \mathbf{v} \otimes \mathbf{v}\right) = \nabla \sigma + \mathbf{S}_l, \tag{2}$$

$$\frac{\partial \left(\rho e_t\right)}{\partial t} + \nabla \left(\rho e_t \mathbf{v} - \mathbf{v}\sigma + \mathbf{q}\right) = S_j + \mathbf{S}_r, \tag{3}$$

where ρ stands for the gas density, $\mathbf{v}$ gas velocity, σ stress tensor, and e_t the total specific energy. Equations (1)-(3) are coupled with a low-frequeny electromagnetic approximation [5] for the electric potential (4) and magnetic vector potential (5)

$$\nabla \times \frac{1}{\mu} \nabla \times \mathbf{A} + \sigma \frac{\partial \mathbf{A}}{\partial t} = -\sigma \nabla \Phi + \mathbf{J}, \tag{4}$$

$$-\nabla \cdot \left(\sigma \nabla \Phi\right) = \nabla \cdot \left(\sigma \frac{\partial \mathbf{A}}{\partial t}\right) + \nabla \cdot \mathbf{J}, \tag{5}$$

where μ stands for the magnetic permeability, σ electrical conductivity, $\mathbf{J}$ electric current density, $\mathbf{A}$ magnetic vector potential, and $\mathbf{\Phi}$ electric potential. The equations are coupled through the source term for Lorentz force density $\mathbf{S}_l = \mathbf{J} \times \mathbf{B}$, the temperature and pressure dependencies of the material data, and the Ohmic heating source density $S_j = \mathbf{J} \cdot \mathbf{E}$. By definition $\mathbf{B} = \nabla \times \mathbf{A}$, $\mathbf{E} = -\nabla \mathbf{\Phi}$, and $\mathbf{J} = \sigma \mathbf{E}$ are given, where $\mathbf{E}$ represents the electric field.

An ideal gas model is used and turbulence is modeled using the k-ϵ approach. Thermodynamic properties, transport coefficients, and spectral data for air are provided in [6]. The transport coefficients for electrical conductivity, thermal conductivity and dynamic viscosity are calculated as a function of temperature and pressure. The ideal gas is assumed to be compressible. Thus, the density is calculated as a function of temperature, pressure and velocity with respect to the ideal gas law. The relative permeability for air and copper is assumed to be $\mu_r = 1$ and the electrical conductivity of copper is set to $\sigma_{\mathrm{Cu}} = 59.6\,\mathrm{MS/m}$. The convective heat transfer between gas and solid components is not considered and a constant wall temperature of $300\,\mathrm{K}$ is defined.

Calculating the source term for radiation heat flux $\mathbf{S}_r$ the discrete ordinate method is used (see, e.g., [7]). The absorption spectrum is divided into six bands, as described in [1]. Besides, the Hybrid mean is used to calculate the temperature and pressure dependent absorption coefficients for each band [8]. The arc is initialized as a cylindrical channel of an increased electrical conductivity profile and a Gaussian distribution with the highest value of $\sigma = 5.7 \cdot 10^7\,\mathrm{S/m}$ in the center.
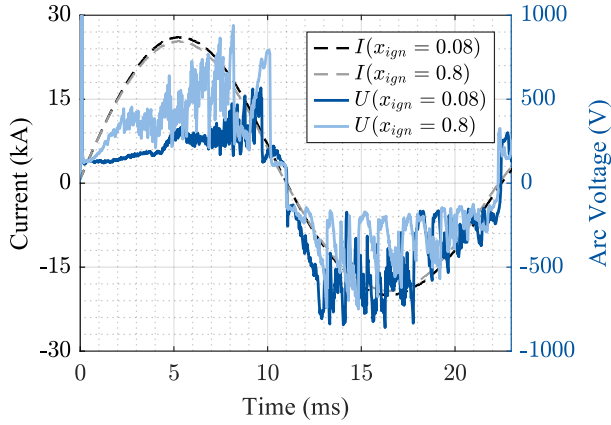
The ablation and erosion models for polymer and

Figure 2. Current and arc voltage measurements for ignition locations at $x_{\mathrm{ign}} = 0.08\,m$ and $x_{\mathrm{ign}} = 0.8\,m$.
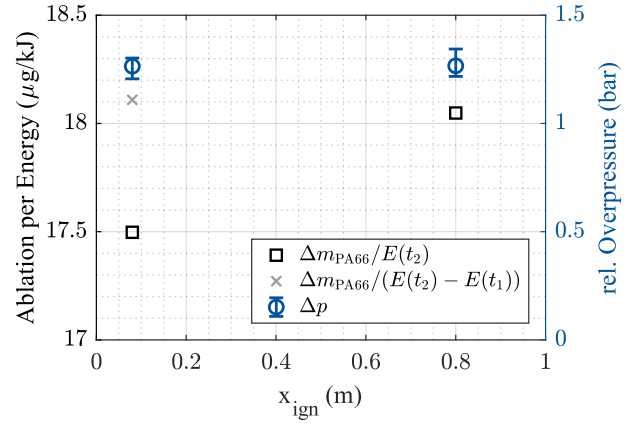

Figure 3. Mass loss-to-energy ratio and pressure build-up composed of the measurements of the test series for ignition locations at $x_{\mathrm{ign}} = 0.08\,m$ and $x_{\mathrm{ign}} = 0.8\,m$.

copper are neglected, since they have not been parameterized yet for fault arc applications. Effects at the arc roots, such as anode and cathode fall voltages, are neglected for the time being, as these are not parameterized for fault arc simulations either.

The governing equations for fluid dynamics, electric potential, and radiative heat transfer are solved using the finite volume method (FVM). Because of the ferromagnetic materials, the finite element method (FEM) is used to solve for the magnetic vector potential. The model is discretized using a polyhedral mesh for the FVM and a tetrahedral mesh for the FEM solver. In the FVM mesh, Prism layers are included at the boundaries between gaseous and solid regions. The electric current density is mapped onto the FE mesh using nearest neighbor interpolation after each FV time step. Conversely, the magnetic field density is mapped after each FE time step.

3. Results and Discussion

In the following, exemplary results for two ignition locations ($x_{\mathrm{ign}} = 0.08\,\mathrm{m}$ and $x_{\mathrm{ign}} = 0.8\,\mathrm{m}$) for a fault time of $t = 70\,\mathrm{ms}$ are presented. The parameters are set to $d_{\mathrm{bb}} = 0.03\,\mathrm{m}$, $d_{\mathrm{be}} = 0.055\,\mathrm{m}$, and $d_{\mathrm{dp}} = 0.05\,\mathrm{m}$. Polyamid 66 (PA 66) is used as polymer, while the busbars are made from copper. The system is filled with air at atmospheric pressure. In Figure 2 the infeed current, which is used as a boundary condition in the simulation, and the arc voltage are shown. As can be seen, the arc itself has a negligible influence on the current. After ignition an instant rise in the arc voltage to $300\,\mathrm{V}$ for $x_{\mathrm{ign}} = 0.8\,\mathrm{m}$ can be seen. Whereby the arc voltage for $x_{\mathrm{ign}} = 0.08\,\mathrm{m}$ remains at $120\,\mathrm{V}$ to $180\,\mathrm{V}$ until $t_1 = 4\,\mathrm{ms}$. This is due to the distance the arc moves, without significant magnetic widening, between both busbars. Although both arcs are expanding repetitively after t_1, the voltage peak values differ up to $400\,\mathrm{V}$. Two potential factors may account for the observed disparity. Firstly, when ignition takes place directly at $x_{\mathrm{ign}} = 0.8\,\mathrm{m}$, the rapid rise in temperature within the surrounding gas takes place

directly at the end of the busbars. This facilitates expansion of the arc, resulting in an increased arc voltage. Secondly, it allows for a greater initial ablation of PA 66, which diminishes the electrical conductivity of the gas and consequently contributes to an increased arc voltage. For times greater $10\,\mathrm{ms}$, the voltages are in good comparison. Additionally, it is evident that the voltage collapses to an approximately constant level of $\pm 200\,\mathrm{V}$ every few microseconds, indicating the re-ignition of the fault arc between the busbars.

Figure 3 shows the results for PA 66 ablation and pressure build-up during the fault arc event. To evaluate the ablation, the total mass loss is normalized by the total arc energy converted in a series of tests. It is evident that ignition in front of the PA 66 plates results in a higher ratio of ablation per energy. The total mass loss within a test series for ignition at the start and end of the busbars is $10.53\,\mathrm{g}$ and $11.23\,\mathrm{g}$, respectively. By disregarding the energy input of the arc from ignition to reaching the end of the busbars, difference in the mass loss-to-energy ratio between the two test series is only $0.34\,\%$. This result shows the need to include arc movement in the studies and the influence on ablation depending on how long the arc remains in the immediate vicinity of polymers, since the mass loss-to-energy remains constant. Comparing all three pressure build-up results, with the horizontal lines marking the minimum and maximum values, it is apparent that the pressure increase is nearly identical for both configurations. Hence, it can be inferred that different factors contribute to the similar pressure build-up. Igniting the arc at $x_{\mathrm{ign}} = 0.08\,\mathrm{m}$ leads to a greater distance traveled by the arc through the surrounding gas, resulting in enhanced convection and therefore heat transfer to the surrounding gas. Conversely, ignition at $x_{\mathrm{ign}} = 0.8\,\mathrm{m}$ leads to a larger PA 66 ablation, due to the higher amount of energy converted in the vicinity of the polymer, which also contributes to the observed pressure build-up.
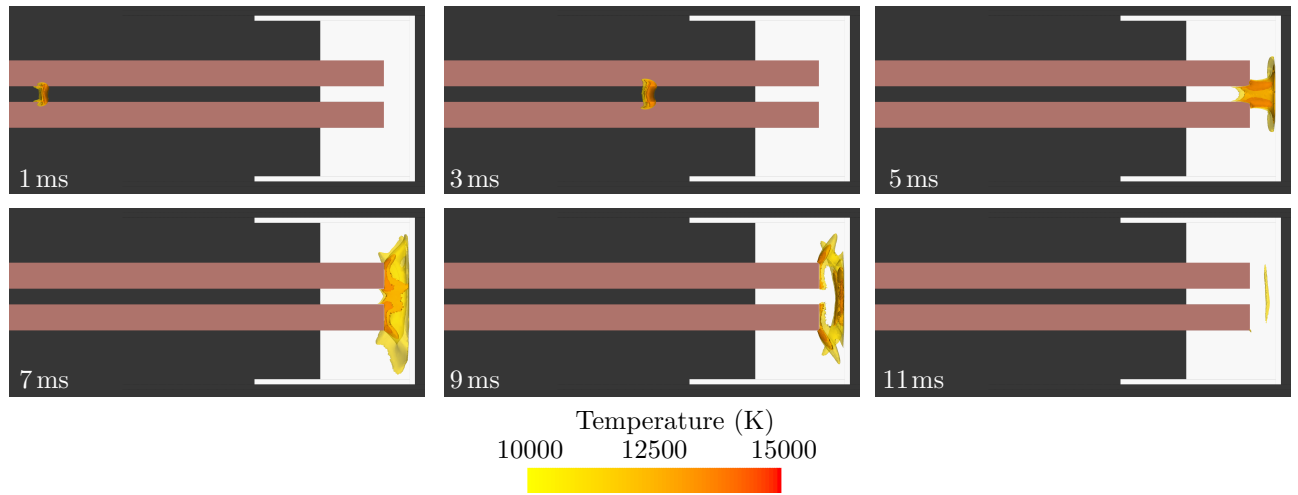
Figure 4. Examplary arc shape represented as temperature-isosurfaces for the first 11 ms for ignition location at $x_{\mathrm{ign}} = 0.08\,m$.

Figure 4 shows exemplary the momvement of the arc after ignition at $x_{\mathrm{ign}} = 0.08\,\mathrm{m}$ until the first current zero crossing. In the first 4 ms the arc moves along the busbars, accelerated by the Lorentz forces. At 5 ms the arc extends beyond the end of the busbars and burns onto the right polymer wall. The arc root advances to the upper and lower edge of the electrodes over the next 4 ms. The current zero crossing is reached at 11 ms. As a result, the arc temperature falls almost completely below 10 000 K. Figure 5 shows the comparison between experimental and simulative arc voltage and pressure build-up, for the first 35 ms. Taking into account the disregarded fall voltages, PA 66 ablation and copper erosion, the voltage prediction for ignition at $x_{\mathrm{ign}} = 0.08\,\mathrm{m}$ demonstrates satisfactory agreement with experimental results, whereby the simulated voltage is on average too low. However, for ignition at $x_{\mathrm{ign}} = 0.8\,\mathrm{m}$, the arc voltages deviate significantly in the first 10 ms, indicating an higher influence of the disregarded phenomena, including ablation and erosion effects. In the initial 4 ms the predicted voltage rises considerable steeper. Afterwards, the arc collaps and re-ignites close to the initial ignition position leading to the comparable low arc voltage in the subsequent period. Overall the arc dynamics indicated by the voltage progression over time can not be predicted by the simulation, showing a need for further investigation.

For better comparison, the same Savitzky-Golay-Filter is applied on the simulated pressure curve. In general, the simulated pressure build-up is in good agreement with the experimental results for both ignition locations, with the deviation increasing from 20 ms for $x_{\mathrm{ign}} = 0.08\,\mathrm{m}$. Moreover, the simulation model is able to predict the disparities in pressure build-up during the initial half-oscillation between the arc propagating along the busbars and the one expanding directly at the end of the busbars.
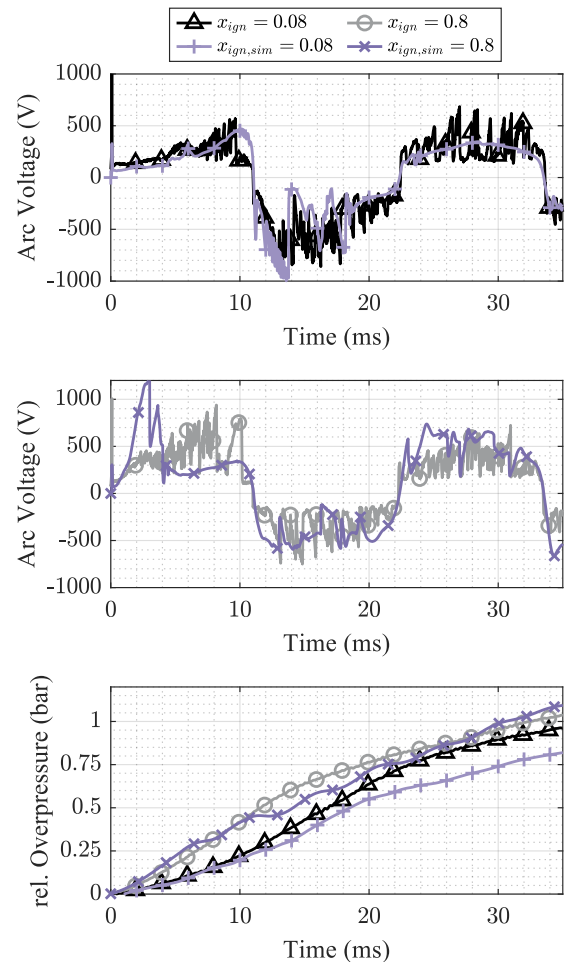

Figure 5. Simulative and experimental results of arc voltage and relative overpressure for the first 35 ms for ignition locations at $x_{\mathrm{ign}} = 0.08\,m$ and $x_{\mathrm{ign}} = 0.8\,m$.

4. Conclusion

In this paper, an experimental setup for investigating fault arcs and validating fault arc simulations is presented. The setup is modular, allowing different

boundary conditions to be altered in order to investigate the effects on the fault arc. Exemplary, the influence of different ignition locations on the arc voltage, pressure build-up, and polymer ablation is investigated. The results are discussed for the ignition location $x_{\mathrm{ign}} = 0.08\,\mathrm{m}$ and $x_{\mathrm{ign}} = 0.8\,\mathrm{m}$, respectively. It can be seen that igniting the arc at the end of the busbars leads to a higher arc voltage and polymer ablation. Furthermore, the total pressure build-up is almost identical, indicating the complex interactions between different mechanisms contributing to the pressure build-up. The measurements for arc voltage and pressure build-up are compared to first simulative results, showing good agreement regarding the pressure build-up for both configurations. Comparing the arc voltages it can be noticed that the simulation is not yet capable to predict the high arc dynamics. Conversely, the arc movements between the busbars can be predicted in good agreement, which could be used in the future to predict the migratory behavior in switchgear. However, further investigation is needed, as well as consideration of modeling approaches for ablation and erosion processes.

Acknowledgements

References

[1] C. Rümpler. *Lichtbogensimulation für Niederspannungsschaltgeräte*. Dissertation, Technische Universität Ilmenau, Ilmenau, 2009.

[2] F. Reichert, J.-J. Gonzalez, and P. Freton. Modelling and simulation of radiative energy transfer in high-voltage circuit breakers. *IEEE Transactions on Plasma Science*, 45(37):375201, 2012. `doi:10.1088/0022-3727/45/37/375201`.

[3] C. Rümpler and V. R. T. Narayanan. Arc modeling challenges. *Plasma Physics and Technology*, 2:261–270, 2015.

[4] S. Singh, D. S. Thevar, and O. Granhaug. Internal arc root movement and burnthrough prediction by simulation using first principle. In *CIRED 2021 - The 26th International Conference and Exhibition on Electricity Distribution*, pages 35–40. Institution of Engineering and Technology, 2021. ISBN 978-1-83953-591-8. `doi:10.1049/icp.2021.1849`.

[5] A. Gleizes, J. J. Gonzalez, and P. Freton. Thermal plasma modelling. *Journal of Physics D: Applied Physics*, 38(9):R153–R183, 2005. `doi:10.1088/0022-3727/38/9/R01`.

[6] Y. Cressault, S. Kimpeler, and A. Moser. Thermophysical properties of Air-PA66-Cu plasmas in DC-contactors: Unpublished. Paper accepted. *Plasma Physics and Technology*, 2023.

[7] M. F. Modest. *Radiative Heat Transfer*. Academic Press, New York, third edition edition, 2013. ISBN 0123869447.

[8] S. Kozu, T. Fujino, T. Yoshino, and T. Mori. Radiative transfer calculation of CO_2 thermal plasma using a hybrid plack–rosseland mean absorption coefficient. *Proceedings of the 22nd international conference on gas discharges and their applications*, pages 127–130, 2018.